NJC

ROYAL SOCIETY OF CHEMISTRY

PAPER

View Article Online
View Journal | View Issue

Cite this: *New J. Chem.*, 2024, **48**, 11606

Macrophage-red blood cell hybrid membrane-coated ultrasound-responsive microbowls to eliminate pathogens, endotoxins, and heavy metal ions from blood†

Jianxing Jing,[a] Mingchen Lv,[a] Wei Hu,[a] Runxin Teng,[a] Zhenghong Ge,[a] Peng Wu,[b] Yao Zhang,*[a] Min Sun*[c] and Zhen Fan*[a]

Sepsis is a potentially life-threatening condition triggered by pathogens such as bacteria and toxins. In clinical settings, hemoperfusion has been used as a therapeutic technique for the treatment of sepsis to remove pathogens, toxins and other inflammatory mediators from the bloodstream. However, the existing adsorption process of hemoperfusion is not specific to sepsis-related pathogens or toxins, resulting in unsatisfactory removal effectiveness and the lack of capture selectivity. Herein, we developed an ultrasound-responsive asymmetric polymeric microbowl coated with macrophage and red blood cell (RBC) membranes to selectively eliminate pathogens, toxins, and heavy metal ions from blood. Poly(glycidyl methacrylate) spherical microparticles were first synthesized and then eroded using dibutyl phthalate and styrene to form a microbowl structure. This asymmetric structure could provide acoustic radiation pressure gradients to realize orientation motion under non-invasive ultrasound fields with a velocity of 37.14 μm s^{-1} at 20 V_{p-p}, which could increase adsorption efficiency in physiological environments by fuel-free programable movements. In addition, the macrophage and RBC membrane coating endowed the microbowl with desired biocompatibility, enhanced blood circulation and the ability to selectively eliminate endotoxins, bacteria and heavy metal ions. Endotoxin removal assay showed that 92.80% of endotoxin was eliminated within 15 minutes. Owing to the affinity between the red blood cell membrane and heavy metal ions, the removal efficiency reached 92.75% and 93.91% for Pb^{2+} and Hg^{2+}, respectively. Meanwhile, over 90% of *S. aureus* in the blood was eliminated owing to the selective recognition and adhesion of bacteria by macrophage membrane proteins. Overall, this work on ultrasound-responsive asymmetric polymeric microbowls provides a new insight to eliminate pathogens, toxins and heavy metal ions from the bloodstream for sepsis treatment.

Received 17th February 2024,
Accepted 15th May 2024

DOI: 10.1039/d4nj00783b

rsc.li/njc

1. Introduction

Sepsis, also referred to as blood poisoning, is a classic disease that is characterised by the dysregulation of the body's response to infection and leads to organ dysfunction, thereby threatening the lives of approximately 50 million people each year.[1,2] Patients with sepsis usually require blood purification such as hemoperfusion to remove pathogens and related toxins.[3–5] Localized infection and pathogen entry into the bloodstream would activate certain pattern recognition receptors on the surface of immune cells and lead to an overwhelming and dysregulated inflammatory reaction throughout the body.[6] Additionally, heavy metal ions, such as lead and mercury, can augment the expression of pro-inflammatory cytokines through various mechanisms, alongside the generation of reactive oxygen species, thereby exacerbating the inflammatory response.[7–9] As a commonly applied approach for sepsis treatment, hemoperfusion is a technique for blood purification that restores physiological functions by adsorbing harmful components in the blood through hemoperfusion adsorbents in perfusion columns.[10] Current hemoperfusion adsorbents are typically composed of activated carbon or resin, both of which offer a large surface area for the physical adsorption of toxins.[11] Recently, protein materials have paved a novel path in the

[a] *Department of Polymeric Materials, School of Materials Science and Engineering, Tongji University, 4800 Caoan Road, Shanghai 201804, China. E-mail: 20310062@tongji.edu.cn, fanzhen2018@tongji.edu.cn*
[b] *Department of Orthopedics, Shanghai Tenth People's Hospital, Shanghai 200072, China*
[c] *Department of Gynaecology and Obstetrics, Shanghai Fourth People's Hospital, School of Medicine, Tongji University, Shanghai 200434, China. E-mail: 22310108@tongji.edu.cn*

† Electronic supplementary information (ESI) available: Fig. S1–S10 (SEM, fluorescence spectra, *etc.*). See DOI: https://doi.org/10.1039/d4nj00783b

design of novel hemoperfusion adsorbents.[12,13] Yang *et al.* developed a biocompatible protein–polysaccharide complex that exhibited multiple-removal ability for liver and kidney metabolic wastes, toxic metal ions, and antibiotics, which has significantly promoted the development and applications of protein materials in hemoperfusion adsorbents.[14] Nowadays, the development of hemoperfusion adsorbents with high removal efficiency and excellent selective adsorption is particularly crucial.[15] Therefore, it would be of great value to develop a new approach of blood purification to specifically and efficiently eliminate bacteria, endotoxins, and heavy metal ions for enhanced therapeutic outcomes.[16]

To increase the adsorption efficiency, self-propelled nano/microparticles guided by external fields have been applied to remove contaminants such as micro/nanoplastics, organic molecules, and oil spills.[17] For example, Katherine *et al.* developed $BiVO_4$ microparticles to achieve individual and collective swimming under visible light irradiation, which could selectively adhere with yeast cell walls for fungicidal activity.[18] In addition, Qiu *et al.* synthesized asymmetric magnetic mesoporous silica nanobottles loaded with Fe_3O_4 nanoparticles to effectively adsorb and remove heavy metal ions with precise directional control and recyclability under external magnetic fields.[19] Compared to the previously reported light and magnetic field as driving forces, ultrasound (US) has been widely applied clinically in a non-invasive manner, which could ensure cellular and tissue integrity with enhanced penetration into deeper tissues and navigation under intricate physiological environments.[20] In addition, compared to isotropic symmetric micro/nanoparticles, micro/nanoparticles with asymmetric structures exhibit different properties in a single particle, such as polar and non-polar, hydrophilic and hydrophobic, and anionic and cationic owing to their non-uniform shapes and surface properties,[21,22] which makes it possible to precisely control and direct movements under external fields in clinical settings. Currently, multiple approaches have been developed to fabricate asymmetric microstructures. Most of them were fabricated by template-assisted electrodeposition. For example, Ahmed *et al.* reported asymmetric metallic and bimetallic nanorods fabricated by electrochemical deposition within the pores of anodic alumina membranes.[23] He *et al.* reported asymmetric ultrasound-driven nanoswimmers with gold-nanoshell-functionalized multilayer tubular structures using a template-assisted electrodeposition protocol.[24] For polymer-based asymmetric nanoparticles, our groups have previously synthesized and manipulated the opening concaves of nanobowls *via* optimizing hydrogen bonding and π–π interactions during the homopolymer self-assembly[25] and co-assembly of homopolymers and peptides.[26] However, the existing asymmetric micro/nanoparticles are primarily designed to enhance the movement efficiency, which lack desired bioactivity for biomedical applications.

To endow nanomaterials with designated biofunctions, functionalization with various cell membranes containing a series of membrane proteins has been reported. Zhang *et al.* developed biodegradable polymeric nanoparticles coated with natural RBC membranes to enhance their circulation time for cargo delivery through bypassing macrophage uptake and systemic clearance.[27] Wang *et al.* designed macrophage membrane-coated gold–silver nanocages for efficient bacterial targeting and serving as a drug delivery vehicle, demonstrating improved bacterial adherence, prolonged circulation, and excellent biocompatibility.[28] Recent studies have begun to shed light on the synthesis, characterization, and applications of asymmetric micro/nanoparticles coated with cell membranes.[29] Such hybrid nanomaterials leverage the inherent characteristics of both components, allowing for tailored functionalities and enhanced performance in bioapplications such as drug delivery, biosensing, and targeted therapeutics. For instance, He *et al.* developed near-infrared light-powered Janus mesoporous silica nanoparticles coated with macrophage cell membranes for active targeting cancer cells and thermomechanical perforation of cancer cell membranes.[30] However, biofunctionalization of asymmetric polymeric micro/nanoparticles remains an area with limited exploration but holds immense promise.

In this work, we developed an ultrasound-driven asymmetric microbowl coated with hybrid cell membranes to scavenge endotoxins, bacteria and some heavy metal ions (Pb^{2+} and Hg^{2+}). The asymmetric structure of the polymeric microbowl was transformed from poly(glycidyl methacrylate) (PGMA) microspheres. The microspheres were prepared by dispersion polymerization and then the surfaces of the microspheres were eroded by dibutyl phthalate and styrene to form an asymmetric bowl-like structure. The outside diameter of the microbowl was ~1.3 μm and the inside opening diameter was ~500 nm. The RBC membrane was isolated from erythrocytes using the hypotonic treatment method, and the macrophage cell membrane was extracted from RAW 264.7 *via* a repeated freeze-thawing process. The RBC and macrophage cell membranes were co-encapsulated onto the surface of the microbowls by repeated extrusion of 3 μm-porous membranes through a mini-extruder with the same membrane protein content. The movement of this polymeric microbowl could be initiated and controlled under an ultrasound field at 1.46 MHz, and its velocity was affected by the amplitude of the sinusoidal ultrasound with the highest speed of 37.14 μm s^{-1} at 20 V_{p-p}. Heavy metal ions were adsorbed and removed by attaching to the RBC membrane proteins coated on the microbowl surface.[31–33] The clearance efficiency of Pb^{2+} and Hg^{2+} was more than 90% respectively. Meanwhile, macrophage membrane proteins could specifically recognize and adhere to endotoxins and bacteria, which resulted in a bacteria removal rate of over 90%. In general, this ultrasound-driven membrane-coated microbowl demonstrated an effective approach to scavenge endotoxins, bacteria and some heavy metal ions during hemoperfusion.

2. Experimental

2.1. Materials

Glycidyl methacrylate (GMA, 99%), azobisisobutyronitrile (AIBN), polyvinylpyrrolidone (PVP), dibutyl phthalate (99%), sodium

dodecyl sulfate (SDS), styrene (99.5%) and anhydrous ethanol were used without further purification. $HgCl_2$, $PbCl_2$, methanol, dioxane and sodium hydroxide (NaOH) were purchased from Shanghai Aladdin Biochemical Technology Co., Ltd. Phosphate buffered saline (PBS) and Tris–magnesium buffer (TM buffer) were purchased from Beyotime Biotech. Inc. L02 liver cells and L929 cells were obtained from the Institute of Biochemistry and Cell Biology, Chinese Academy of Sciences (Shanghai, China). Cell Proliferation and Cytotoxicity Assay (CCK-8) Kit, fluorescein isothiocyanate (FITC), rhodamine B and Coomassie Brilliant Blue G-250 were purchased from Beijing Solarbio Science & Technology Co., Ltd (Beijing, China). Water was processed using a Millipore purification system (Darmstadt, Germany) with a minimum resistivity of 18.2 MΩ cm.

2.2. Synthesis of PGMA seed microspheres

PGMA seed microspheres were prepared *via* dispersion polymerization.[34] Briefly, 4.0 g of PVP was dissolved adequately in anhydrous ethanol and double-distilled water mixed solutions in 10/1 volume ratio. Then, 300 mg of AIBN dissolved in 2.0 g of GMA was then added. After purging for 20 min with nitrogen, the system was heated to 70 °C for 12 h of reaction. The obtained product was washed three times with ethanol and double-distilled water. Finally, the residue was freeze-dried to obtain the PGMA seed microspheres.

2.3. Fabrication of microbowls

First, 50 mg of PGMA seed microspheres were dispersed in 5 mL of 2.5 wt% SDS aqueous solution under magnetic stirring. Subsequently, 250 mg of dibutyl phthalate and 250 mg of styrene were added. After being eroded at 40 °C for 24 h, the microbowls were obtained and purified by centrifugation and lyophilization.

2.4. Extraction of the red blood cell (RBC) membrane

The RBC membrane was obtained by hypotonic treatment from 4% mouse erythrocyte.[35] The RBC was washed with ice-cold PBS, obtained by centrifuging at 700*g* for 5 min at 4 °C, and then treated with an ice-cold hypotonic buffer (10% PBS) at 4 °C for 6 h to burst the RBC membrane. Unbroken RBCs were then removed by centrifugation at 1000*g* for 10 min. The remaining supernatant was centrifuged at 14 000*g* for 30 min to obtain the pink RBC membrane. The protein content in the RBC membrane was determined by the Bradford protein assay (Shanghai Sangon Biotech. Co. Ltd, China). The obtained RBC membrane was stored at −80 °C for later study.

2.5. Extraction of the macrophage cell membrane

The macrophage cell membrane was isolated from RAW 264.7 cells as previously reported with slight modifications.[36] In brief, RAW 264.7 cells were cultured and harvested at a concentration of 5×10^7 cells per mL by centrifugation. The cells were resuspended and incubated for 15 min in an ice-cold Tris–magnesium buffer (TM buffer, pH = 7.4, 50 mM Tris–HCl, 8 mM $MgSO_4$) containing a protease inhibitor. Cells were fragmented by a repeated freeze-thawing process. Then, the cell homogenate was centrifuged at 700*g* at 4 °C for 10 minutes to remove the unbroken cells and nuclei. The supernatant was centrifuged at 14 000*g* at 4 °C for 30 min to obtain the macrophage membranes. The cell membrane fragments were washed by centrifugation at 14 000*g* at 4 °C and redispersed in 1 mL PBS solution. The protein content in the purified macrophage membrane was also determined by the Bradford protein assay. The obtained macrophage membrane was stored at −80 °C for later study.

2.6. Measurement of the membrane protein content

The protein content of the RBC membrane and macrophage membrane was measured by the Bradford protein assay.[37] First, 20 μL of BSA solutions with different concentrations (20, 40, 60, 80, 100, and 150 μg mL^{-1}) were added into a 96-well plate. Then, 200 μL Coomassie Brilliant Blue G-250 solution was added and incubated for 10 min. The same 20 μL of RBC membrane or macrophage membrane solutions were incubated with 200 μL Coomassie Brilliant Blue G-250 solution. The absorbances of all samples were detected using a UV-Vis microplate reader. The membrane concentrations were calculated based on the calibration curve of standard samples.

2.7. Fabrication of RBC-MP-microbowls

RBC-MP-microbowls were prepared by enclosing microbowls with the obtained RBC membrane and macrophage membrane. In brief, two kinds of membranes were fused in PBS in 1/1 protein weight ratio under ultrasonication (42 kHz, 200 W) for 10 min. Furthermore, microbowls were incubated with hybrid membranes under ultrasonication for another 10 min and subsequently extruded through 3.0 μm polycarbonate porous membranes for 20 times using an Avanti mini extruder. The resulting RBC-MP-microbowls were washed three times with PBS and obtained by centrifugation at 5000 rpm.

2.8. Characterization of RBC-MP-microbowls

Scanning electron microscopy (SEM). The morphologies of PGMA microspheres, microbowls and RBC-MP-microbowls were characterized using a Zeiss Sigma 300 VP instrument. Images were recorded with the secondary electron mode at 2–5 kV.

Confocal laser scanning microscopy (CLSM). Rhodamine B-labelled RBC membranes and FTIC-labelled macrophage cell membranes were observed using a Nikon Ti2 confocal laser scanning microscope (Nikon, Japan).

Optical microscopy. The movement of the microbowl was recorded using an Olympus BX60 optical microscope.

A Microplate Reader (Multiskan™FC, Thermo Fisher Scientific) was used to perform the Bradford assay and confirm the cell viability.

Fluorescence spectroscopy. Fluorescence emission spectra of RBC-MP-microbowls and microbowls were measured using a Fluorescence Spectrophotometer F-4700 (Hitachi, Ltd, Japan). The excitation and emission slit widths were both set to 5 nm. The scan speed was set to 60 nm min^{-1}. Fluorescence emission spectra were recorded at a fixed time interval.

Inductively coupled plasma-optical emission spectrometer (ICP-OES). To evaluate the heavy metal removal efficiency of RBC-MP-microbowls, the concentrations of heavy metal ions (Hg^{2+} and Pb^{2+}) were measured by ICP-OES (PerkinElmer 8300).

Fluorescence microplate reader. The relative fluorescence unit of different samples was measured using a multiple microplate reader of Infinite 200pro (Tecan Austria GmbH). The excitation wavelength and emission wavelength were set at 360 nm and 465 nm with an emission bandwidth of 35 nm.

2.9. Cell membrane detection of RBC-MP-microbowls

To confirm that the hybrid membrane encapsulated the microbowls successfully, the protein content of the RBC-MP-microbowls was quantitatively measured by the Bradford assay (Shanghai Sangon Biotech. Co. Ltd, China). In brief, the microbowls (1 mg mL^{-1}) and RBC-MP-microbowls (1 mg mL^{-1}) were centrifuged and washed three times with PBS. Subsequently, 20 μL of the microbowls (1 mg mL^{-1}) and RBC-MP-microbowls (1 mg mL^{-1}) were mixed with 200 μL Coomassie Brilliant Blue G-250 solution. After 10 min incubation, the absorbance was detected and the protein contents were calculated based on the calibration curve of standard samples. Additionally, the membrane protein series of both hybrid membranes and RBC-MP-microbowls were compared with sodium dodecyl sulfate-polyacrylamide gel electrophoresis (SDS-PAGE) protein characterization. The samples were heated at 100 °C for 5 min and run at 180 V for 45 min, followed by Coomassie Blue staining overnight. After washing, the final image was captured and recorded.

To further confirm the presence of the hybrid membranes onto the surface of the microbowls, the RBC membrane and macrophage membrane were labelled with rhodamine B (excitation/emission = 546/568 nm) and FITC (excitation/emission = 495/525 nm) respectively before coating onto the microbowls. The fluorescence images were acquired using a CLSM with a 10× microscope eyepiece and a 60× microscope objective.

2.10. Acoustic propulsion studies

The acoustic equipment to propel the RBC-MP-microbowls was built with reference to previous work.[24] A rectangle cell (10 mm × 10 mm) was home-made by applying two layers of polyimide Kapton tape (50 μm thickness per layer) to a conductive glass slide (40 mm × 40 mm × 2 mm). The solution in the cell was excited by a piezoelectric ceramic disc transducer affixed to the conductive glass slide parallel to the acoustic cell (Shenzhen Huajingda Electronics Co., Ltd, catalog no. H4P163000). The piezoelectric ceramic was connected to a function generator system, including a signal generator (FEEL TECH Inc., FY2300) and a signal amplifier (FEEL TECH Inc., FYA2010s).

The Olympus BX60 optical microscope and a commercial video-capturing camera were used for observing the movements of RBC-MP-microbowls and recording videos. Videos of motion were taken at 400× magnification at a frame rate of 25 s^{-1}. The motion was tracked using a Video Spot Tracker. The speed was calculated by dividing the displacement of the microbowl centre between two frames by the time interval, and then the average of the speed over the selected tracking period was taken. The tracking was repeated with multiple microbowls to ensure statistically robust results. We verified the velocity of the microbowls in whole blood with reference to previous work.[38] We replaced the liquid environment with whole blood spiked with anticoagulants and compared the velocity of microbowls with that in PBS.

2.11. *In vitro* cell viability assay

A CCK-8 assay was performed to assess the microbowls against L929 and B16 cells. Briefly, approximately 1.0×10^5 cells per well with an MEM medium were seeded into 96-well plates. After culturing for 24 h, the primary MEM medium was replaced with a medium containing microbowls (0, 62.5, 125, 250, 500, and 1000 μg mL^{-1}) at designated concentrations for another 24 h. Then, 20 μL of CCK-8 solution was then fed into each well, incubating for an additional 1 h. The absorbance of each sample was measured using a microplate reader at 450 nm. The cell viability was calculated according to the following formula:

$$\text{Cell viability (\%)} = \frac{[OD_{450}(\text{sample}) - OD_{450}(\text{blank})]}{[OD_{450}(\text{control}) - OD_{450}(\text{blank})]} \times 100\%$$

2.12. Hemolysis assay

Hemolysis assays were performed in accordance with a previously published method. First, 2.0 mL fresh blood was drawn from mouse eyes and centrifuged (3000 rpm for 10 min), and then RBCs were resuspended in PBS to prepare a washed RBC suspension. The cells were exposed to water and different concentrations of RBC-MP-microbowls (0, 12.5, 25, 50 and 100 μg mL^{-1}) for 30 min. After that, the mixture was centrifuged for 10 min at 4 °C, and the absorbance of the supernatant was measured using a microplate reader at an absorbance wavelength of 560 nm. The degree of hemolysis was calculated using the following formula:

$$\text{Hemolysis (\%)} = \frac{[OD_{560}(\text{sample}) - OD_{560}(\text{blank})]}{[OD_{560}(\text{water}) - OD_{560}(\text{blank})]} \times 100\%$$

2.13. Removal of heavy metal ions using RBC-MP-microbowls

The performance of RBC-MP-microbowls for the removal of heavy metal ions was evaluated using aqueous solutions containing Pb^{2+} and Hg^{2+} (~10 mg L^{-1}), respectively. The concentration of heavy metal ions in a solution was measured using an Inductively Coupled Plasma-Optical Emission Spectrometer (ICP-OES, PerkinElmer 8300). Briefly, 100 μL of RBC-MP-microbowls (5 mg mL^{-1}) were added to 1 mL of aqueous solutions containing metal ions. In order to verify the effect of motion excited by US on the removal of heavy metal ions, another set with the same conditions was treated with US. As a control, 100 μL of deionized water was added to 1 mL of aqueous solutions containing metal ions. After adsorption for 1 h, the concentration of ions in the supernatant obtained by centrifugation and filtration through a poly(ether sulfone) (PES, 0.22 μm) membrane was measured by ICP-OES. Each set was repeated three times.

Similarly, the adsorption efficiencies of RBC-MP-microbowls were investigated for different concentrations of heavy metal ions to better study their adsorption capacity for Pb^{2+} and Hg^{2+}. The ion concentrations were set at 100–200 μg L^{-1} for Pb^{2+} and 50–150 μg L^{-1} for Hg^{2+}. The setting ranges for these concentrations are based on the safe concentrations for heavy metal poisoning.[39,40] The heavy metal ion concentrations of samples before and after adsorption were determined by ICP-OES.

2.14. Removal of endotoxins using RBC-MP-microbowls

The performance of RBC-MP-microbowls in endotoxin removal was evaluated by a Recombinant Factor C Endpoint Fluorescent Assay. First, the standard curve was fitted with standard samples ranging from 0.005 EU per mL to 5 EU per mL to determine the correspondence between relative fluorescence unit (ΔRFU) and endotoxin concentration. The ΔRFU was determined using a fluorescence Microplate Reader (Tecan Austria GmbH). ΔRFU was calculated using the following equation:

$$\Delta RFU = RFU_{T=1h} - RFU_{T=0}$$

After that, 100 μL of RBC-MP-microbowls (5 mg mL^{-1}) were mixed with 900 μL of endotoxin solution (~3 EU per mL) for different incubation periods (15, 30, 45, and 60 min). The same 100 μL of DI water was mixed with 900 μL of endotoxin solution (~3 EU per mL) as the control set. The RFU was recorded at T = 0 and T = 1 h respectively. The corresponding endotoxin concentration was calculated using the fitted standard curves. The role of US on endotoxin adsorption was similarly investigated by setting ion concentrations of 0.5 and 1.0 EU per mL and with and without US conditions.

2.15. Binding and isolation of macrophage-adhering bacteria

The bioactivity of RBC-MP-microbowls was assessed in binding and isolation of bacteria using *Staphylococcus aureus* (*S. aureus*, ATCC 29213) as model bacteria.[41] *S. aureus* was cultured in a Luria-Bertani medium (LB medium, 0.10 g mL^{-1}) in an oven at 37 °C for 12 h. The bacterial suspension (100 μL) was added into the PBS (9.9 mL) to make a diluted bacterial suspension. Then, 100 μL of RBC-MP-microbowls (5 mg mL^{-1}) were mixed with the above-mentioned bacterial suspension (900 μL). Similarly, 100 μL of PBS was mixed with the bacterial suspension (900 μL) and set as the control group. After the US incubation for 3 h in a US field (1.46 MHz, 20.0 V_{p-p}), bacterial suspensions from different groups were spread onto plates to continue incubation for 12 h, and then colony growth was recorded.

3. Results and discussion

3.1. Preparation and characterization of RBC-MP-microbowls

The RBC-MP-microbowls were prepared in two stages of evolving PGMA microspheres to microbowls and hybrid cell membrane encapsulation, as illustrated in Fig. 1. Previous work had reported that the asymmetric structure would be beneficial for ultrasound-induced propulsion.[23] However, it is still challenging to prepare asymmetric microparticles with an adjustable concave size. In order to prepare asymmetric micro/nanoparticles, the PGMA microspheres were first fabricated by dispersion polymerization. The spherical morphology with an average diameter of approximately 1.14 μm was observed using an SEM (Fig. 2A and Fig. S1, ESI†). Afterwards, a bowl-like structure was prepared by an eroding strategy with dibutyl phthalate and styrene. In the presence of surfactant sodium dodecyl sulfate, organic droplets composed of dibutyl phthalate and styrene adsorbed onto the surface of PGMA microspheres.[42] Gradually, the organic phase eroded the surface of the microspheres, creating a concave shape and ultimately forming a unique bowl-like structure (Fig. 2B). The outer diameter of the microbowl was approximately 1.29 μm and the inner diameter was approximately 562.5 nm (Fig. S2, ESI†).

After the asymmetric microbowl was prepared, the hybrid cell membrane was coated onto microbowls using an Avanti mini extruder. The RBC membrane was isolated from erythrocytes using the hypotonic treatment method,[43] and the macrophage cell membrane was extracted from RAW 264.7 *via* a repeated freeze-thawing process.[36] Additionally, the membrane protein contents of RBC membranes and macrophage membranes (Fig. S3, ESI†) were 122.27 μm mL^{-1} and 87.99 μm mL^{-1}, respectively. The RBC-MP hybrid membranes were prepared in 1/1 protein weight ratio. After incubation for 20 min, the RBC-MP hybrid membranes and microbowls were extruded through polycarbonate porous membranes for 20 times with 1 mg mL^{-1} of total membrane proteins. A sodium dodecyl sulfate-polyacrylamide gel electrophoresis (SDS-PAGE) assay was then performed to compare the protein type in the RBC membranes, macrophage membranes, RBC-microbowls, MP-microbowls and RBC-MP-microbowls. As shown in Fig. 2C, while a negligible protein signal was found in the bare microbowls, the protein composition in the RBC-MP hybrid membrane was primarily retained in the RBC-MP-microbowls. In order to characterize the fusion and coating level of hybridized membranes onto microbowls, fluorescein isothiocyanate (FITC) and rhodamine B were used to label the macrophage and red blood cell membranes, respectively. The fluorescence emission spectra of RBC-MP-microbowls demonstrated that rhodamine B and FITC were successfully labelled to the cell membrane, as shown in Fig. S4 (ESI†). Then, hybrid membrane-coated microbowls were imaged using a confocal laser scanning microscope (CLSM) to further verify the coating efficiency (Fig. 2D). Both green fluorescence (FITC representing the macrophage membrane) and red fluorescence (rhodamine B representing the red blood cell membrane) were observed from the microbowls, demonstrating the desired hybrid cell membrane coating.

3.2. Regulating effect on microbowls

The morphology and structure of the microbowls were related to the erosive action of dibutyl phthalate and styrene. Corresponding microbowls were prepared at different mass ratios of dibutyl phthalate and styrene (DS ratios), and the microstructures were characterized by SEM. Compared to PGMA microspheres (Fig. 3A), the diameter of the denting opening

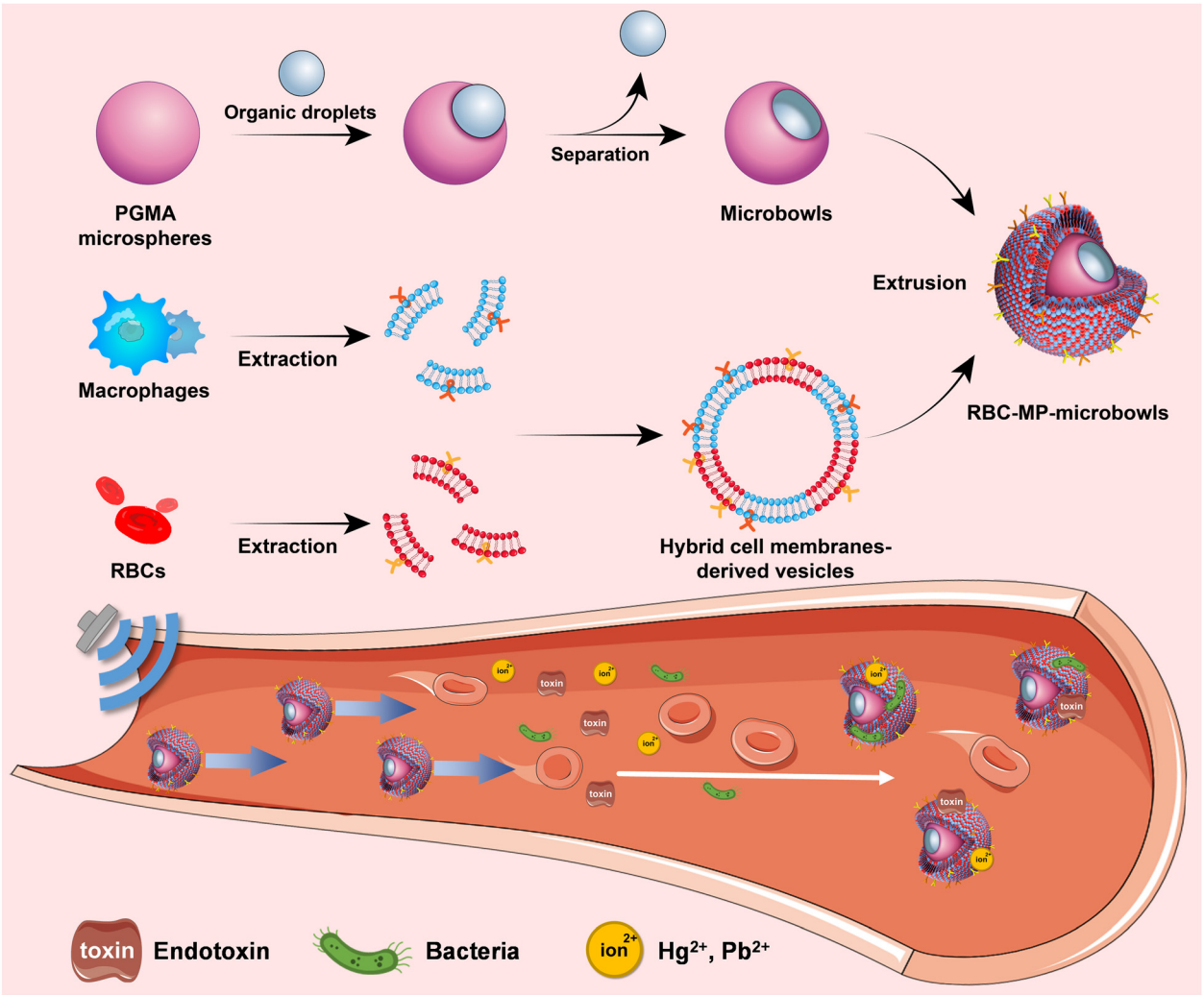

Fig. 1 Schematic illustration of the preparation of macrophage-red blood cell hybrid membrane-coated ultrasound-responsive microbowls and the process of eliminating pathogens, endotoxins, and heavy metal ions for blood purification.

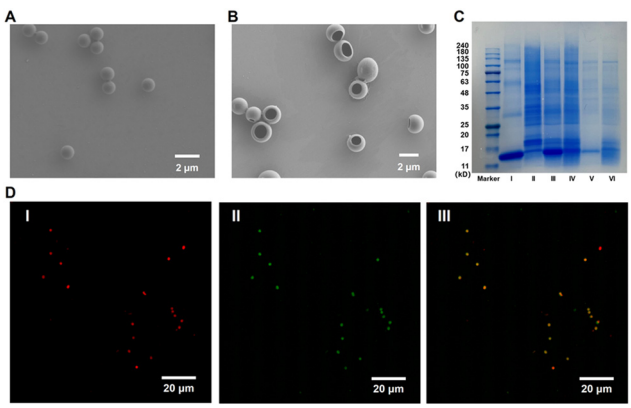

Fig. 2 Characterizations of RBC-MP-microbowls. (A) SEM image of PGMA seed microspheres. (B) SEM image of the microbowls. (C) Protein profiles of the RBC membranes (I), macrophage membrane (II), RBC-MP hybrid membranes (III), RBC-MP-microbowls (IV), RBC-microbowls (V) and MP-microbowls (VI) determined using an SDS-PAGE electrophoresis assay. (D) CLSM images of RBC-MP-microbowls.

ranged from 586.2 nm to 2.9 μm with the increase in styrene ratio (Fig. 3B–D). Moreover, excessive styrene gradually increased the diameter of the openings and eventually the bowl-like structure could not be maintained. In addition, the SEM images of different dibutyl phthalate contents with the same styrene contents were also acquired, and are shown in Fig. S5 (ESI†). Although the DS ratio was obviously changed from 5.0 mg/5.0 mg to 10.0 mg/5.0 mg, there were no significant changes in the microstructure, demonstrating that dibutyl phthalate has less impact on the morphology change towards microbowls. Bowl-like structures prepared at various eroding times were also investigated, and the corresponding SEM images are displayed in Fig. S6 (ESI†). After 3 h of reaction, only a small concave was observed (Fig. S6A, ESI†). With the continuous erosion by dibutyl phthalate and styrene, a typical bowl-like structure was formed after 12 h of reaction. However, the bowl-like structure became unstable and distorted when the reaction time reached 36 h (Fig. S6D, ESI†).

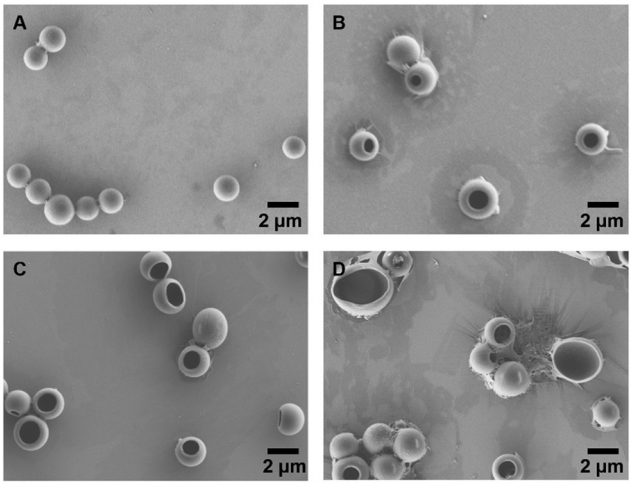

Fig. 3 SEM images of microbowls prepared with different DS ratios. (A) DS ratio = 0/0; (B) DS ratio = 5.0 mg/5.0 mg; (C) DS ratio = 5.0 mg/10.0 mg; and (D) DS ratio = 5.0 mg/15.0 mg (per 1 mg PGMA seed microspheres). Scale bar = 2 μm.

3.3. Ultrasound responsibility and propulsion performance of RBC-MP-microbowls

The ultrasound-induced propulsion indexes of the RBC-MP-microbowls, such as movement trajectories and velocities, were studied using an optical microscope and a video tracking software Video Spot Tracker (Version 8.01). The frequency of the RBC-MP-microbowls in response to ultrasound stimulation was investigated, and it was found to be capable of directional motion at a frequency of 1.46 MHz. Previous studies have demonstrated that ultrasound could form standing waves and generate the primary acoustic radiation force perpendicular to the levitation plane, which suspended the microbowls. In addition, the second acoustic radiation force and streaming-induced drag force were generated in the levitation plane.[44] The shape and structure asymmetry caused the asymmetric distribution of two forces and acoustic radiation pressure gradients to realize orientation motion under non-invasive ultrasound fields.[45]

Then, the moving trajectories in a period of 5 s under different ultrasound amplitudes (5 V_{p-p}, 10 V_{p-p}, 15 V_{p-p}, and 20 V_{p-p}) were captured. Corresponding captured movements at 5 V_{p-p} and 10 V_{p-p} were recorded, and are shown in ESI,† Movies S1 and S2, respectively. In Fig. 4A, the motion trajectories are illustrated at different ultrasound amplitudes with obvious directional movements. The corresponding trajectories and direction of movement were recorded and normalized, as shown in Fig. 4B, by recording the coordinate points. Besides, the moving trajectories without ultrasound were captured, which showed relatively irregular movement attributed to the Brownian motion. The linearity of the trajectories indicated the stability of the directional movement of microbowls. The mean square displacements (MSD) were calculated by accumulating the squared linear distance between two frames, and are shown in Fig. 4C. As the ultrasound amplitude increased from 5 to 20 V_{p-p}, the MSD raised from 7.58 μm^2 to 186.8 μm^2, indicating

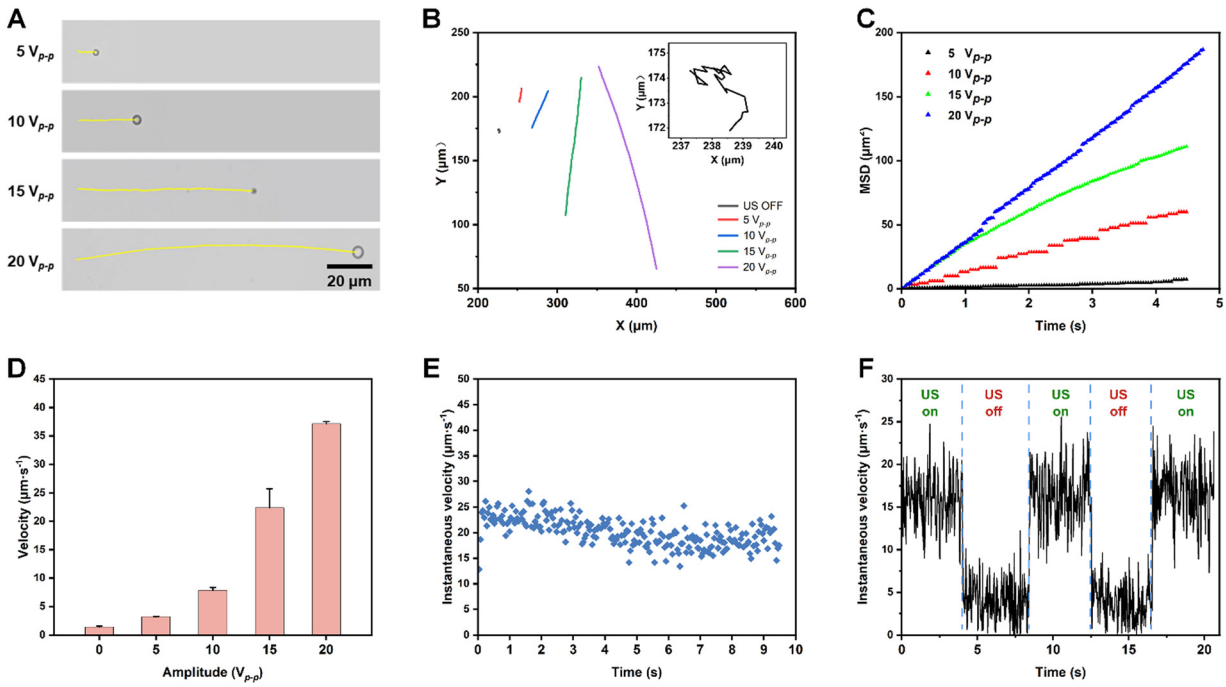

Fig. 4 Characterizations of the ultrasound-induced directional movements of the RBC-MP-microbowls: (A) a series of images captured at 5 s intervals showing the movement at different ultrasound amplitudes (5–20 V_{p-p}). Scale bar = 20 μm. (B) Corresponding tracking trajectory of the RBC-MP-microbowls during 5 s at different ultrasound amplitudes (0–20 V_{p-p}). (C) Average MSD *versus* time interval analysed from tracking trajectories. (D) Dependence of the average velocity of RBC-MP-microbowls in 5 s at different ultrasound amplitudes. (E) Instantaneous velocity of RBC-MP-microbowls at 15 V_{p-p} analysed from the tracking trajectory. (F) Responsiveness of instantaneous velocity to ultrasound analysed *via* ultrasound ON/OFF.

a correlation between the moving velocity and the ultrasound amplitude. The mean velocities with different ultrasound amplitudes were measured to assess the effect on motion velocity (Fig. 4D). The mean velocity at 0, 5 V_{p-p}, 10 V_{p-p}, 15 V_{p-p} and 20 V_{p-p} was 1.43 μm s^{-1}, 3.18 μm s^{-1}, 7.84 μm s^{-1}, 22.39 μm s^{-1} and 37.14 μm s^{-1}, which exponentially increased ($Y = 1.40947 \times 1.17777^{X}$, Fig. S7, ESI†).

To study the velocity of the RBC-MP-microbowl in solutions with different viscosities, PBS and whole blood spiked with anticoagulants were used under ultrasound. As shown in Fig. S8 (ESI†), the velocities of RBC-MP-microbowls in PBS and whole blood were 37.14 μm s^{-1} and 29.45 μm s^{-1}, respectively. In addition, red blood cells did not show any obvious ultrasound-responsive movement, which is in accordance with the existing results reported in the literature.[46] Overall, it has been demonstrated that the RBC-MP-microbowls could realize ultrasound propulsion in blood with reduced velocity compared to that in PBS.

To verify the persistence and stability of ultrasonic-responsive motion, the motion of the RBC-MP-microbowls was monitored at 15 V_{p-p} for 10 s, and the instantaneous velocities were measured by calculating the linear displacement between two frames. As shown in Fig. 4E, the instantaneous velocities were mainly between 20 μm s^{-1} and 25 μm s^{-1} in the first 4 s and then slightly decreased in the following 6 s, indicating that the ultrasound-propulsion movement had desired persistence and stability. In addition, the motion of RBC-MP-microbowls was further examined with frequent ultrasound switch (on and off), and instantaneous velocities were analysed to verify their transient responsiveness (Fig. 4F and Movie S3, ESI†). It showed that when the ultrasound switched from "on" to "off" or from "off" to "on", the instantaneous velocity changed instantaneously. Almost all the erythrocytes retained their biconcave disc shape after ultrasound stimulation, which is within the range of ultrasound frequency (<5 MHz) in clinical settings, which also verified the biosafety of sonication.[47,48] Besides, the movements at an ultrasound frequency of 1.46 MHz were recorded in the simultaneous presence of erythrocytes and RBC-MP-microbowls (Movie S4, ESI†). The RBC-MP-microbowls moved normally in the environment, while no obvious movements of erythrocytes were observed, demonstrating the selective ultrasound propulsion towards RBC-MP-microbowls.

3.4. Biocompatibilities and biofunctions of RBC-MP-microbowls

Mouse fibroblast (L929) and B16 cell lines were selected to evaluate the biocompatibility of RBC-MP-microbowls by a CCK-8 assay. As shown in Fig. 5A, the cell viability was higher than 95% after co-culturing with 200 μg mL^{-1} of RBC-MP-microbowls for 24 h. In addition, we investigated the hemolytic property by incubation of RBC-MP-microbowls and RBCs. There was no apparent hemolysis phenomenon observed (Fig. 5B), demonstrating the feasibility of microbowls used during hemoperfusion.[49]

Endotoxin is one of the important pathogenic components causing sepsis. A recombinant factor c endpoint fluorescent assay was performed to evaluate the endotoxin removal efficiency of RBC-MP-microbowls. As shown in Fig. 5C and Fig. S9 (ESI†), after incubation with ~2.5 EU per mL endotoxin for 15 min, the concentration of endotoxin significantly decreased to 0.53 EU per mL. The endotoxin removal efficiency was calculated with 79.6% calculated according to the calibration curve (Fig. S10, ESI†). We also investigated the removal ability with or without ultrasound at 0.5 and 1.0 EU per mL initial ion concentrations. As shown in Fig. 5D and E, the concentrations of endotoxin were significantly reduced with RBC-MP-microbowl treatment. Furthermore, with RBC-MP-microbowls under ultrasound stimulation, the removal efficiency further increased from 80.55% to 92.80% at 1.0 EU per mL.

To verify the ability of scavenging heavy metal ions of the RBC-MP-microbowls, Pb^{2+} and Hg^{2+} (~10 mg L^{-1}) were selected as common blood contaminants.[31–33] In detail, 100 μL of RBC-MP-microbowls (242.75 μg mL^{-1} of membrane protein) were added to 1 mL of heavy metal ion solutions with or without sinusoidal ultrasound at 1.46 MHz. As shown in Fig. 5F, the concentration of Pb^{2+} was reduced from 14.84 mg L^{-1} to 4.11 mg L^{-1} after incubation with RBC-MP-microbowls, which further decreased to 2.34 mg L^{-1} under ultrasonic stimulation of 1.46 MHz. Similarly, the concentration of Hg^{2+} was reduced from 13.01 mg L^{-1} to 3.68 mg L^{-1}, and further decreased to 2.33 mg L^{-1} under ultrasonic stimulation of 1.46 MHz. The RBC-MP-microbowls reached removal efficiencies of 84.2% for Pb^{2+} and 82.1% for Hg^{2+} (Fig. 5G). Meanwhile, the adsorption capacity in removing Pb^{2+} and Hg^{2+} could reach 25.00 mg g^{-1} and 21.36 mg g^{-1}, respectively. According to clinical reports, the reference values of blood lead concentration and serum mercury concentration were <50 μg L^{-1} [39] and <15 μg L^{-1},[40] respectively. Therefore, we investigated the adsorption efficiency for different above-threshold concentrations of Pb^{2+} and Hg^{2+} with RBC-MP-microbowl + US treatment. As shown in Fig. 5H and I, the highest removal efficiency of RBC-MP-microbowls could reach 92.75% and 93.91%, respectively. This demonstrated that the RBC-MP-microbowls possessed great removal capacities for Pb^{2+} and Hg^{2+}, which was attributed to the adsorption of the RBC membrane protein to heavy metal ions[50] and ultrasound-propelling-boosted scavenging ability.[51]

Besides, the ability of scavenging bacteria was investigated using a *Staphylococcus aureus* (*S. aureus*) model. As shown in Fig. 5J, the removal efficiency for *S. aureus* was up to 96.7% in the RBC-MP-microbowl + US group, which was more effective than that of the PBS + US group and RBC-MP-microbowls, indicating the synergetic effects of the macrophage membrane and ultrasound-induced movements for bacterial scavenging. The function of adsorption to endotoxins and bacteria of RBC-MP-microbowls was attributed to the recognition and adsorption of macrophage cell membrane proteins (such as Toll-like receptors, NOD-like receptors, and cluster of differentiation 14[52]) to endotoxins and bacteria. In addition, ultrasound promoted the movement of RBC-MP-microbowls, ultimately reaching great removal efficiencies for endotoxins and bacteria.

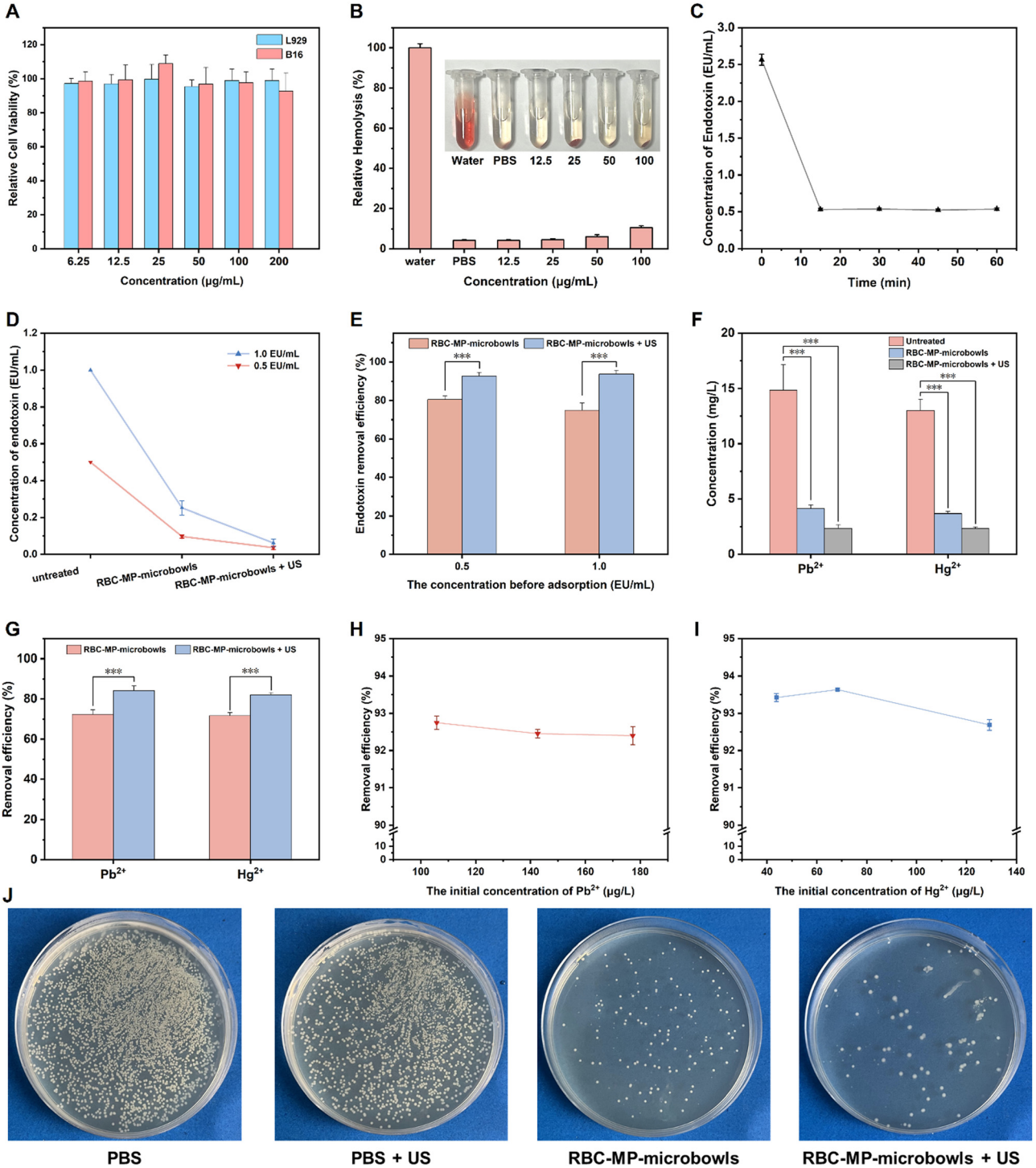

Fig. 5 Characterization of the bioactivity and ability to adsorb and remove the RBC-MP-microbowls: (A) cell viability assessment after incubation with different concentrations of RBC-MP-microbowls for 24 h. (B) Hemolysis activity of the RBC-MP-microbowls at different concentrations. (C) Concentration of endotoxins after incubation with the RBC-MP-microbowls for different times. (D) Concentrations of endotoxins before and after adsorption by the RBC-MP-microbowls with or without US. (E) Removal efficiency of endotoxins at different initial endotoxin concentrations. (F) Concentrations of heavy metal ions before and after adsorption. (G) Removal efficiency of the heavy metal ions. (H) Pb^{2+} removal efficiencies at different initial adsorption concentrations. (I) Hg^{2+} removal efficiencies at different initial adsorption concentrations. (J) Removal effect of *S. aureus* with the RBC-MP-microbowls under ultrasound stimulation. The statistical significance was analysed using Student's *t*-test. *: $P < 0.05$; **: $P < 0.01$; ***: $P < 0.001$.

4. Conclusions

In this study, we have developed a strategy to prepare ultrasound-responsive asymmetric polymeric microbowls coated with cell membranes to eliminate endotoxins, heavy metal ions and bacteria. The microbowls showed a unique asymmetric structure that enabled orientation motion under non-invasive ultrasound fields, which could achieve 37.14 μm s^{-1} at 20 V_{p-p} under fuel-free programable sonication. The utilization of the macrophage and RBC hybrid membranes on microbowls enhanced their biocompatibility and offered desired bioactivities. In detail, macrophage membranes facilitate the selective recognition and adhesion of pathogens and endotoxins. Experimental data revealed that 92.80% of endotoxin and over 90% of *S. aureus* in blood were eliminated. Additionally, the affinity between the RBC membrane and heavy metal ions contributes to the efficient removal of contaminants such as Pb^{2+} (92.75% removal efficiency) and Hg^{2+} (93.91% removal efficiency). Overall, our ultrasound-responsive asymmetric polymeric microbowls represented a promising advancement for blood purification during sepsis treatments.

Author contributions

Jianxing Jing: conceptualization, formal analysis, investigation, writing, review and editing. Mingchen Lv: editing. Wei Hu: editing. Runxin Teng: editing. Zhenghong Ge: editing. Yao Zhang: review and editing, supervision. Min Sun: review and editing, supervision. Zhen Fan: writing—original draft preparation, writing—review and editing, supervision.

Conflicts of interest

There are no conflicts of interest to declare.

Acknowledgements

This research was supported by National Natural Science Foundation of China (52222306, 22075212, and 22305177), Shanghai international scientific collaboration fund (23520 710900), the fellowship of China Postdoctoral Science Foundation (2022M720107, GZB20230517) and Shanghai ''Super Postdoc'' Incentive Plan (2022568), Shanghai Rising-Star Program (Sailing, 23YF1433000), Natural Science Foundation of Shanghai (20ZR1443200). The tracking software Video Spot Tracker was developed by the CISMM at the University of North Carolina at Chapel Hill.

References

1 K. E. Rudd, S. C. Johnson, K. M. Agesa, K. A. Shackelford, D. Tsoi, D. R. Kievlan, D. V. Colombara, K. S. Ikuta, N. Kissoon, S. Finfer, C. Fleischmann-Struzek, F. R. Machado, K. K. Reinhart, K. Rowan, C. W. Seymour, R. S. Watson, T. E. West, F. Marinho, S. I. Hay, R. Lozano, A. D. Lopez, D. C. Angus, C. J. L. Murray and M. Naghavi, *Lancet*, 2020, **395**, 200–211.
2 T. van der Poll, M. Shankar-Hari and W. J. Wiersinga, *Immunity*, 2021, **54**, 2450–2464.
3 X. Y. Wang, Z. P. Xia, H. L. Wang, D. Wang, T. W. Sun, E. Hossain, X. Pang and Y. F. Liu, *Theranostics*, 2023, **13**, 3224–3244.
4 A. Jörres, *Crit. Care*, 2018, **22**, 357.
5 M. Fisher, L. Golestaneh, M. Allon, K. Abreo and M. H. Mokrzycki, *Clin. J. Am. Soc. Nephrol.*, 2020, **15**, 132–151.
6 K. L. Christman, *Nat. Biomed. Eng.*, 2023, **7**, 92–93.
7 H. Mei, P. L. Yao, S. S. Wang, N. Li, T. F. Zhu, X. F. Chen, M. M. Yang, S. Zhuo, S. T. Chen, J. M. Wang, H. Wang, D. Xie, Y. N. Wu and Y. Y. Le, *Toxicol. Sci.*, 2017, **159**, 327–338.
8 A. Goutam Mukherjee, U. Ramesh Wanjari, K. Renu, B. Vellingiri and A. Valsala Gopalakrishnan, *Environ. Toxicol. Pharmacol.*, 2022, **92**, 103859.
9 M. Boskabady, N. Marefati, T. Farkhondeh, F. Shakeri, A. Farshbaf and M. H. Boskabady, *Environ. Int.*, 2018, **120**, 404–420.
10 X. Ye, Y. Yu, C. Yang, Q. Fan, L. Shang and F. Ye, *J. Colloid Interface Sci.*, 2022, **624**, 546–554.
11 S. Q. Wu, P. P. Yue, Y. S. Ma, Y. K. Zou, W. J. Liang and Q. F. Ye, *Adv. Mater.*, 2023, 2305152.
12 L. Li, Y. Zhang, Y. Wu, Z. Wang, W. Cui, C. Zhang, J. Wang, Y. Liu and P. Yang, *Adv. Funct. Mater.*, 2024, 2315509.
13 Y. Liu, S. Miao, H. Ren, L. Tian, J. Zhao and P. Yang, *Nat. Protoc.*, 2024, **19**, 539–564.
14 M. Li, M. Chen, F. Yang, R. Qin, Q. Yang, H. Ren, H. Liu and P. Yang, *Adv. Healthcare Mater.*, 2023, **12**, 2300999.
15 Y. Xu, Y. Li, W. Zhao and C. Zhao, *J. Colloid Interface Sci.*, 2023, **631**, 231–244.
16 L. Papafilippou, A. Claxton, P. Dark, K. Kostarelos and M. Hadjidemetriou, *Adv. Healthcare Mater.*, 2021, **10**, 2001378.
17 M. Urso, M. Ussia and M. Pumera, *Nat. Rev. Bioeng.*, 2023, **1**, 236–251.
18 K. Villa, F. Novotný, J. Zelenka, M. P. Browne, T. Ruml and M. Pumera, *ACS Nano*, 2019, **13**, 8135–8145.
19 B. Qiu, L. Xie, J. Zeng, T. Liu, M. Yan, S. Zhou, Q. Liang, J. Tang, K. Liang and B. Kong, *Adv. Funct. Mater.*, 2021, **31**, 2010694.
20 D. Q. Huang, J. L. Wang, C. H. Song and Y. J. Zhao, *Innovation*, 2023, **4**, 100421.
21 A. K. Pearce, T. R. Wilks, M. C. Arno and R. K. O'Reilly, *Nat. Rev. Chem.*, 2021, **5**, 21–45.
22 H. T. Li, L. Chen, X. M. Li, D. G. Sun and H. J. Zhang, *Nano-Micro Lett.*, 2022, **14**, 45.
23 S. Ahmed, W. Wang, L. J. Bai, D. T. Gentekos, M. Hoyos and T. E. Mallouk, *ACS Nano*, 2016, **10**, 4763–4769.
24 W. Wang, Z. G. Wu, X. K. Lin, T. Y. Si and Q. He, *J. Am. Chem. Soc.*, 2019, **141**, 6601–6608.
25 H. Sun, D. Liu and J. Du, *Chem. Sci.*, 2019, **10**, 657–664.

26 S. Lin, H. Sun, E. J. Cornel, J. H. Jiang, Y. Q. Zhu, Z. Fan and J. Z. Du, *Chin. J. Polym. Sci.*, 2021, **39**, 1538–1549.
27 C. M. J. Hu, L. Zhang, S. Aryal, C. Cheung, R. H. Fang and L. F. Zhang, *Proc. Natl. Acad. Sci. U. S. A.*, 2011, **108**, 10980–10985.
28 C. Wang, Y. Wang, L. Zhang, R. J. Miron, J. Liang, M. Shi, W. Mo, S. Zheng, Y. Zhao and Y. Zhang, *Adv. Mater.*, 2018, **30**, 1804023.
29 W. Lee, L. Ha, D.-P. Kim and J. Kim, *J. Colloid Interface Sci.*, 2022, **623**, 54–62.
30 M. Xuan, J. Shao, C. Gao, W. Wang, L. Dai and Q. He, *Angew. Chem., Int. Ed.*, 2018, **57**, 12463–12467.
31 X. Y. Guo, W. J. Wang, X. H. Yuan, Y. Yang, Q. H. Tian, Y. Xiang, Y. Sun and Z. M. Rai, *J. Colloid Interface Sci.*, 2019, **536**, 563–574.
32 A. Hill and J. Gailer, *J. Inorg. Biochem.*, 2021, **216**, 111279.
33 M. M. Wan, T. T. Xu, B. Chi, M. Wang, Y. Huang, Q. Wang, T. Li, W. Q. Yan, H. Chen, P. Xu, C. Mao, B. Zhao, J. Shen, H. Xu and D. Q. Shi, *Angew. Chem., Int. Ed.*, 2019, **58**, 10582–10586.
34 W. L. Zhang, S. H. Piao and H. J. Choi, *J. Colloid Interface Sci.*, 2013, **402**, 100–106.
35 W. Gao, C. M. J. Hu, R. H. Fang, B. T. Luk, J. Su and L. Zhang, *Adv. Mater.*, 2013, **25**, 3549–3553.
36 C. Gao, Q. X. Huang, C. H. Liu, C. H. T. Kwong, L. D. Yue, J. B. Wan, S. M. Y. Lee and R. B. Wang, *Nat. Commun.*, 2020, **11**, 2622.
37 M. Lv, M. Sun, M. Wu, F. Zhang, H. Yin, Y. Sun, R. Liu, Z. Fan and J. Du, *Nano Lett.*, 2022, **22**, 9621–9629.
38 B. Esteban-Fernández de Ávila, P. Angsantikul, D. E. Ramírez-Herrera, F. Soto, H. Teymourian, D. Dehaini, Y. Chen, L. Zhang and J. Wang, *Sci. Rob.*, 2018, **3**, eaat0485.
39 R. Fuller, P. J. Landrigan, K. Balakrishnan, G. Bathan, S. Bose-O'Reilly, M. Brauer, J. Caravanos, T. Chiles, A. Cohen, L. Corra, M. Cropper, G. Ferraro, J. Hanna, D. Hanrahan, H. Hu, D. Hunter, G. Janata, R. Kupka, B. Lanphear, M. Lichtveld, K. Martin, A. Mustapha, E. Sanchez-Triana, K. Sandilya, L. Schaefli, J. Shaw, J. Seddon, W. Suk, M. M. Téllez-Rojo and C. Yan, *Lancet Planet. Health*, 2022, **6**, e535–e547.
40 Y. Feng and F. Wang, *N. Engl. J. Med.*, 2022, **387**, 1888.
41 R. Teng, Y. Yang, Z. Zhang, K. Yang, M. Sun, C. Li, Z. Fan and J. Du, *Adv. Funct. Mater.*, 2023, **33**, 2214454.
42 L. Tian, X. Li, P. P. Zhao, Z. Ali and Q. Y. Zhang, *Macromolecules*, 2016, **49**, 9626–9636.
43 E. Ben-Akiva, R. A. Meyer, H. Z. Yu, J. T. Smith, D. M. Pardoll and J. J. Green, *Sci. Adv.*, 2020, **6**, eaay9035.
44 W. Wang, L. A. Castro, M. Hoyos and T. E. Mallouk, *ACS Nano*, 2012, **6**, 6122–6132.
45 K. J. Rao, F. Li, L. Meng, H. Zheng, F. Cai and W. Wang, *Small*, 2015, **11**, 2836–2846.
46 Z. Wu, T. Li, J. Li, W. Gao, T. Xu, C. Christianson, W. Gao, M. Galarnyk, Q. He, L. Zhang and J. Wang, *ACS Nano*, 2014, **8**, 12041–12048.
47 E. Jafarzadeh and A. N. Sinclair, *Ultrasound Med. Biol.*, 2019, **45**, 11–20.
48 S. Radjenovic, G. Dörl, M. Gaal and R. Beisteiner, *Brain Sci.*, 2022, **12**, 1277.
49 Z. W. Yin, R. Shi, X. Xia, L. Li, Y. X. Yang, S. K. Li, J. Q. Xu, Y. T. Xu, X. Q. Cai, S. Wang, Z. K. Liu, T. H. Peng, Y. Peng, H. Wang, M. Ye, Y. L. Liu, Z. Chen and W. H. Tan, *Adv. Mater.*, 2022, **34**, 2207870.
50 B. J. Payliss, M. Hassanin and E. J. Prenner, *Chem. Phys. Lipids*, 2015, **193**, 36–51.
51 M. Uygun, B. Jurado-Sánchez, D. A. Uygun, V. V. Singh, L. F. Zhang and J. Wang, *Nanoscale*, 2017, **9**, 18423–18429.
52 K. J. Kieser and J. C. Kagan, *Nat. Rev. Immunol.*, 2017, **17**, 376–390.

